International Journal of Machine Tools & Manufacture 49 (2009) 1136–1143

Contents lists available at ScienceDirect

International Journal of Machine Tools & Manufacture

journal homepage: www.elsevier.com/locate/ijmactool

Continuous model for analytical prediction of chatter in milling

M. Salahshoor [a,*], Hamid Ahmadian [b]

[a] Department of Mechanical Engineering, The University of Alabama, Tuscaloosa, AL 35487, USA
[b] School of Mechanical Engineering, Iran University of Science and Technology, Narmak, Tehran 16844, Iran

ARTICLE INFO

Article history:
Received 28 September 2006
Received in revised form
25 June 2009
Accepted 2 July 2009
Available online 12 August 2009

Keywords:
Euler–Bernoulli Beam
Elastic support
Stability lobe
Tool tuning

ABSTRACT

A novel analytical approach for prediction of chatter in milling process is presented. Existing approaches use lumped-parameter models to define the dynamics of tools/workpieces. In this paper a continuous beam model is employed for prediction of milling operations dynamics. The tool boundary conditions are elastic support at the tool/holder/spindle interface and free support at the other end. Employing the continuous model eliminates the need for tool tip frequency response function (FRF) measurements in tool-tuning practice, especially in micro-milling, where FRF measurement is practically very difficult. Tool/holder/spindle interface parameters, once identified, can be used for other tool lengths. The impact hammer test is used to identify stiffness and damping parameters of the tool/holder/spindle interface. Using the new analytical approach and picking single-frequency solution (SFS), stability lobes are obtained for a slotting operation. The resulting lobes are compared to those obtained by the well-proven lumped-parameter model. In addition to a good general agreement between the two approaches, the continuous model prediction is more conservative for critical depth of cut, which is attributed to its ability to consider all participating modes in the response and so represents a more accurate representation of the system.

1. Introduction

Machine tool chatter is the self-excited relative oscillation between the cutting tool and the workpiece that develops at large metal removal rates. If the closed-loop machining system, which comprises the machine tool structure's dynamics coupled to the cutting process dynamics, dissipates only a portion of the energy provided by the cutting force, then the amplitude of the tool's motion with respect to the workpiece increases to unacceptable levels. Chatter affects adversely both surface finish and dimensional accuracy of the workpiece. Furthermore, it increases tool wear and may cause tool fracture and damage to the machine tool itself. In order to avoid its occurrence conservative metal removal rates are used, thus limiting the efficiency of the metal cutting operations. In order to improve process efficiency, it is vital to identify chatter-free cutting conditions without compromising on metal removal rates. Predictive models are important to industry because in their absence stable cutting conditions are found only through trial and error, which is a costly and time-consuming process [1,2].

Most of the works done in modeling and simulation of chatter phenomenon use a discrete model or the so-called *lumped-parameter model* for representing spindle/holder/tool dynamics at the tool tip [3–15]. The basic idea in a lumped model is the fact that in regenerative chatter mechanism the dynamic behavior of the tool tip plays a dominant role. Hence, spindle/holder/tool assembly can be represented by modal mass, modal stiffness, and modal damping at each of the modes in feed and perpendicular directions. These parameters are extracted from frequency response function (FRF) measurements in each of the two mutually perpendicular directions.

Long, slender end mills are often used in automotive, biomedical, and aerospace industries for macro- [16] or micro-machining [17,18] of components with thin walls, deep pockets, and small internal corner radii. Because of the high flexibility of the tool, most of the deflections encountered during machining are concentrated in the tool. Hence, the spindle/holder assembly can be assumed to be rigid. In the presented continuous model the tool is represented by an Euler–Bernoulli beam and tool/tool holder interface is modeled using a set of translational spring, torsional spring, and hysteretic dampers.

Schmitz [19], Schmitz et al. [20–22], Budak et al. [23], Namazi et al. [24], and Filiz et al. [25] pointed out that changes in tool length, i.e. *tool tuning*, shift the location of stability lobes. Thus, tool length can be used as an optimization parameter to move a highly stable region to the top spindle speed of the machine. Milling simulation requires knowledge of the system dynamics reflected at the tool point. In general, a separate set of tool-point frequency response function measurements must be performed for each tool/holder/spindle combination on a particular machining centre. These measurements can be time consuming, require a trained technician, and lead to costly machine downtime. Besides the foregoing inconveniences, FRF measurement at micro-tool's tip is practically very difficult due to the miniature and slender

* Corresponding author.
E-mail address: msalahshoorpirsoltan@crimson.ua.edu (M. Salahshoor).

0890-6955/$ - see front matter © 2009 Published by Elsevier Ltd.
doi:10.1016/j.ijmachtools.2009.07.016

nature of the latter, which makes it fragile [18]. The continuous model introduced here eliminates this requirement since the tool/holder interface parameters remain unchanged when only tool length is altered. Once the tool/holder/spindle interface parameters are identified, the length of the tool can be tuned in the model to obtain the maximum material removal rate at a specified spindle speed without any need for further FRF measurement at the tool tip.

The rest of this paper is organized as follows. In Section 2, the continuous model of the dynamic milling system is presented. The stability analysis of the dynamic milling process is performed in Section 3 and based on the developed stability procedure the relations between the chatter frequency, depth of cut, and spindle speed are derived. In Section 4, tool/tool holder/spindle interface parameters of the continuous model are identified using the least-squares optimization method and the stability lobes predicted using the continuous beam model on elastic support are presented in Section 5.

2. Dynamic modeling of milling

The continuous model, shown in Fig. 1, has a flexible support representing tool/tool holder/spindle interface at one end, and the cutting force is applied on the other end. The governing equations of motion for the beam based on the Euler–Bernoulli beam theory are

$$EI\frac{\partial^4 \hat{w}_1}{\partial \hat{x}^4}+m\frac{\partial^2 \hat{w}_1}{\partial \hat{t}^2}=0 \tag{1}$$

$$EI\frac{\partial^4 \hat{w}_2}{\partial \hat{x}^4}+m\frac{\partial^2 \hat{w}_2}{\partial \hat{t}^2}=0 \tag{2}$$

The beam parameters are defined as follows: m is the mass per unit length, E the Young's modulus, I the beam cross-section moment of inertia, $\hat{w}_1$ and $\hat{w}_2$ are the transverse displacements in feed and perpendicular to feed directions, respectively, $\hat{x}$ is the tool axial distance from its support, and $\hat{t}$ the time variable.

Boundary conditions of the beam in continuous model in feed and perpendicular directions with the sign convention of positive directions for shear and moment are

$$EI\frac{\partial^3 \hat{w}_1}{\partial \hat{x}^3}(0,\hat{t})+(1+i\eta_{11})k_{11}\hat{w}_1(0,\hat{t})=0,\quad -EI\frac{\partial^3 \hat{w}_1}{\partial \hat{x}^3}(L,\hat{t})=F_1$$
$$EI\frac{\partial^2 \hat{w}_1}{\partial \hat{x}^2}(0,\hat{t})-(1+i\eta_{10})k_{10}\frac{\partial \hat{w}_1}{\partial \hat{x}}(0,\hat{t})=0,\quad \frac{\partial^2 \hat{w}_1}{\partial \hat{x}^2}(L,\hat{t})=0 \tag{3}$$

$$EI\frac{\partial^3 \hat{w}_2}{\partial \hat{x}^3}(0,\hat{t})+(1+i\eta_{21})k_{21}\hat{w}_2(0,\hat{t})=0,\quad -EI\frac{\partial^3 \hat{w}_2}{\partial \hat{x}^3}(L,\hat{t})=F_2$$
$$EI\frac{\partial^2 \hat{w}_2}{\partial \hat{x}^2}(0,\hat{t})-(1+i\eta_{20})k_{20}\frac{\partial \hat{w}_2}{\partial \hat{x}}(0,\hat{t})=0,\quad \frac{\partial^2 \hat{w}_2}{\partial \hat{x}^2}(L,\hat{t})=0 \tag{4}$$

Here k represents the spring constant and η is the hysteretic damping factor. Left subscripts 1 and 2 represent feed and perpendicular directions, respectively. Right subscript 0 represents torsional spring constant or damping factor and right subscript 1 is translational spring constant or damping factor. L is the beam length. F_1 and F_2 are the dynamic milling forces in feed and perpendicular directions, respectively, and are calculated from the following equations:

$$F_1=\sum_{j=1}^{M}-\Lambda_0\{\cos(\phi_j)+r\sin(\phi_j)\}\{\hat{w}_1(L,\hat{t})\sin(\phi_j)+\hat{w}_2(L,\hat{t})\cos(\phi_j)\}g(\phi_j) \tag{5}$$

$$F_2=\sum_{j=1}^{M}-\Lambda_0\{-\sin(\phi_j)+r\cos(\phi_j)\}\{\hat{w}_1(L,\hat{t})\sin(\phi_j)+\hat{w}_2(L,\hat{t})\cos(\phi_j)\}g(\phi_j) \tag{6}$$

$$\Lambda_0=-bK_s(1-e^{-i\omega\tau}) \tag{7}$$

In the above equations b is the chip width, ω the frequency of tool vibration, τ the cutter tooth-passing period, M the number of teeth, K_s the material special cutting force, r the ratio between tangential and radial cutting forces, and $g(\phi_j)$ is a unit pulse function that determines whether the tooth is in or out of cut, i.e.

$$g(\phi_j)=\begin{cases}1, & \phi_e<\phi_j<\phi_a\\ 0 & \text{otherwise}\end{cases},\quad j=1,2,\ldots,M \tag{8}$$

where ϕ_j is the angle of the jth tooth with respect to the perpendicular to the feed direction; ϕ_e and ϕ_a are the entry and exit angles of the cut, respectively. Rewriting Eqs. (5) and (6) in matrix form one arrives at

$$\begin{Bmatrix}F_1\\F_2\end{Bmatrix}=-\Lambda_0\begin{bmatrix}\mu_{11}&\mu_{12}\\\mu_{21}&\mu_{22}\end{bmatrix}\begin{Bmatrix}\hat{w}_1(L,\hat{t})\\\hat{w}_2(L,\hat{t})\end{Bmatrix} \tag{9}$$

where μ^{11}, μ_{12}, μ_{21}, and μ_{22} are as follows:

$$\mu_{11}=\sum_{j=1}^{M}\{\cos(\phi_j)+r\sin(\phi_j)\}\sin(\phi_j)g(\phi_j)$$
$$\mu_{12}=\sum_{j=1}^{M}\{\cos(\phi_j)+r\sin(\phi_j)\}\cos(\phi_j)g(\phi_j)$$
$$\mu_{21}=\sum_{j=1}^{M}\{-\sin(\phi_j)+r\cos(\phi_j)\}\sin(\phi_j)g(\phi_j)$$
$$\mu_{22}=\sum_{j=1}^{M}\{-\sin(\phi_j)+r\cos(\phi_j)\}\cos(\phi_j)g(\phi_j) \tag{10}$$

In the development of the dynamic model it is assumed that the milling operation is slotting with two-flute end mill. This

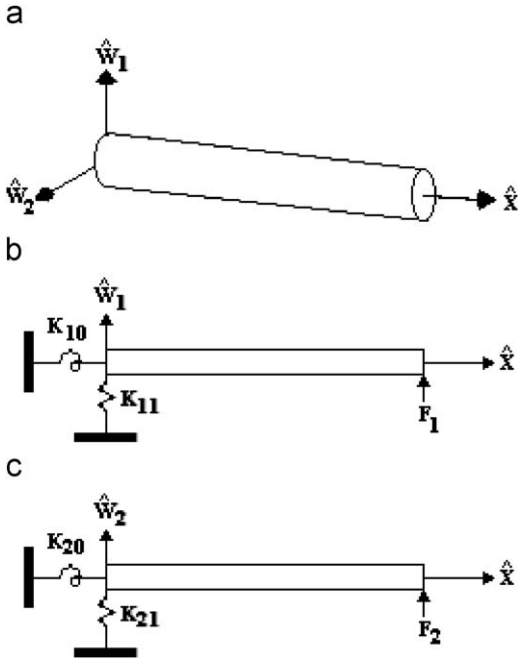

Fig. 1. Continuous model of tool and tool/holder interface.

assumption is made to simplify the cutting force formulation and may be removed by including more terms into the cutting force formulation in Eq. (10) for other applications. The relation between spindle speed (n) and tooth-passing period (τ) for two-flute end mill is as follows:

$$n_{[\mathrm{RPM}]} = \frac{30}{\tau_{[\mathrm{s}]}} \tag{11}$$

As the tool is rotating ϕ_j is a continuous function in time domain, i.e.

$$\phi_1 = \frac{2n\pi}{60}\hat{t} = \pi\left(\frac{\hat{t}}{\tau}\right) \tag{12}$$

$$\phi_2 = \frac{2n\pi}{60}\hat{t} - \pi = \pi\left\{\left(\frac{\hat{t}}{\tau}\right) - 1\right\} \tag{13}$$

Substituting Eqs. (12) and (13) into Eq. (10) and considering the fact that at least one tooth of the cutter is in the cut each time during cutting, i.e. $g(\pi\theta)+g(\pi\theta-\pi) = 1$, one arrives at

$$\begin{aligned}
\mu_{11} &= \{cos(\pi\theta) + r\sin(\pi\theta)\}\sin(\pi\theta),\\
\mu_{21} &= \{-\sin(\pi\theta) + r\cos(\pi\theta)\}\sin(\pi\theta)\\
\mu_{12} &= \{\cos(\pi\theta) + r\sin(\pi\theta)\}\cos(\pi\theta),\\
\mu_{22} &= \{-\sin(\pi\theta) + r\cos(\pi\theta)\}\cos(\pi\theta)
\end{aligned} \tag{14}$$

where $\theta = \hat{t}/\tau$. These are periodic functions of θ and, based on what method is picked in stability analysis, they are approximated in different ways. Stability analysis methods fall into two broad groups of time [5–7,9–14] and frequency [3,4] domain approaches. In the frequency domain approach, periodic functions in Eq. (14) are expanded in a Fourier series and, based on which terms are retained for approximation, multi-frequency solution (MFS) and single-frequency solution (SFS) are sought. In the SFS method, which is applied in this research, only the zero-order term is kept. It is a very practical approach since it gives a closed-form expression for stability boundary. However, this method loses accuracy as the radial immersion decreases and time domain methods like two-stage map [5], temporal FEA [6], or semi-discretization [9] should be implemented to be able to predict both periodic and quasi-periodic chatter. Analyzing stability in the continuous model formulation using the foregoing time domain approaches is under study and does not decrease the importance of continuous models, which eliminate the need for repeated tool tip FRF measurements in tool tuning especially for micro-machining [18]. The zero-order terms or average values of μ_{12}, μ_{12}, μ_{21}, and μ_{22} in their Fourier series expansions are as follows:

$$\begin{aligned}
&\overline{\mu}_{11} = \int_0^1 \mu_{11}\,d\theta, \quad \overline{\mu}_{12} = \int_0^1 \mu_{12}\,d\theta, \quad \overline{\mu}_{21} = \int_0^1 \mu_{21}\,d\theta,\\
&\overline{\mu}_{22} = \int_0^1 \mu_{22}\,d\theta
\end{aligned} \tag{15}$$

These average values are used in Eq. (9) [4]. The next step is to convert the variables of the equations of motion and boundary conditions to a non-dimensional form to simplify the solution procedure. The non-dimensional variables are obtained according to the following scheme:

$$x = \frac{\hat{x}}{L}, \quad w_1 = \frac{\hat{w}_1}{L}, \quad w_2 = \frac{\hat{w}_2}{L}, \quad t = \hat{t}\sqrt{\frac{EI}{mL^4}} \tag{16}$$

Using these variables, one may rewrite Eqs. (1) and (2) as

$$w_1^{\mathrm{iv}} + \ddot{w}_1 = 0 \tag{17}$$

$$w_2^{\mathrm{iv}} + \ddot{w}_2 = 0 \tag{18}$$

where 'iv' and dots denote spatial and time derivatives, respectively. The boundary conditions are also transformed to the following:

$$\begin{aligned}
&w_1'''(0,t) + (1+i\eta_{11})\alpha_{11}w_1(0,t) = 0,\\
&w_1''(0,t) - (1+i\eta_{10})\alpha_{10}w_1'(0,t) = 0\\
&w_1'''(1,t) - \Lambda_1\{\overline{\mu}_{11}w_1(1,t) + \overline{\mu}_{12}w_2(1,t)\} = 0, \quad w_1''(1,t) = 0
\end{aligned} \tag{19}$$

$$\begin{aligned}
&w_2'''(0,t) + (1+i\eta_{21})\alpha_{21}w_2(0,t) = 0,\\
&w_2''(0,t) - (1+i\eta_{20})\alpha_{20}w_2'(0,t) = 0\\
&w_2'''(1,t) - \Lambda_1\{\overline{\mu}_{21}w_1(1,t) + \overline{\mu}_{22}w_2(1,t)\} = 0, \quad w_2''(1,t) = 0
\end{aligned} \tag{20}$$

where

$$\begin{aligned}
&\alpha_{10} = \frac{k_{10}L}{EI}, \quad \alpha_{11} = \frac{k_{11}L^3}{EI}, \quad \alpha_{20} = \frac{k_{20}L}{EI}, \quad \alpha_{21} = \frac{k_{21}L^3}{EI},\\
&\Lambda_1 = \frac{\Lambda_0 L^3}{EI}
\end{aligned} \tag{21}$$

The solution of (17) and (18) satisfying the boundary conditions defined in (19) and (20) represents the dynamic behavior of the tool during milling operations. The following section considers the dynamic behavior of the tool at the chatter frequency.

3. Stability analysis of dynamic milling

According to the linear chatter theory the amplitude of vibration neither increases nor decreases at the limit of stability. Based on this observation, at the stability boundary an undamped solution for the boundary value problem defined in (17) and (18) of the following form is assumed:

$$w_1(x,t) = \varphi(x)e^{i\omega t} \tag{22}$$

$$w_2(x,t) = \psi(x)e^{i\omega t} \tag{23}$$

In the assumed solutions the chatter frequency, ω, is a real-value function. Substituting (22) and (23) in (17) and (18), respectively, and separating the variables, one arrives at the following ordinary differential equations:

$$\varphi^{\mathrm{iv}} - \lambda^4\varphi = 0 \tag{24}$$

$$\psi^{\mathrm{iv}} - \lambda^4\psi = 0 \tag{25}$$

where $\lambda^4 = \omega^2$. The solutions of (24) and (25) are of the following form:

$$\varphi(x) = A_1\sin(\lambda x) + B_1\cos(\lambda x) + C_1\sinh(\lambda x) + D_1\cosh(\lambda x) \tag{26}$$

$$\psi(x) = A_2\sin(\lambda x) + B_2\cos(\lambda x) + C_2\sinh(\lambda x) + D_2\cosh(\lambda x) \tag{27}$$

The coefficients $A_{1,2}$, $B_{1,2}$, $C_{1,2}$, and $D_{1,2}$ are determined by satisfying the boundary conditions. Substituting (22) and (23) into (19) and (20), one obtains the equations that are necessary for determining these coefficients as follows:

$$\begin{aligned}
&\varphi'''(0) + (1+i\eta_{11})\alpha_{11}\varphi(0) = 0, \quad \varphi''(0) - (1+i\eta_{10})\alpha_{10}\varphi'(0) = 0\\
&\varphi'''(1) - \Lambda_1\{\overline{\mu}_{11}\varphi(1) + \overline{\mu}_{12}\psi(1)\} = 0, \quad \varphi''(1) = 0
\end{aligned} \tag{28}$$

$$\begin{aligned}
&\psi'''(0) + (1+i\eta_{21})\alpha_{21}\psi(0) = 0, \quad \psi''(0) - (1+i\eta_{20})\alpha_{20}\psi'(0) = 0\\
&\psi'''(1) - \Lambda_1\{\overline{\mu}_{21}\varphi(1) + \overline{\mu}_{22}\psi(1)\} = 0, \quad \psi''(1) = 0
\end{aligned} \tag{29}$$

The spatial domain functions $\varphi(x)$ and $\psi(x)$ must satisfy the conditions set in (28) and (29). Rewriting these equations in matrix form yields the following homogeneous set of equations:

$$\begin{bmatrix} [M_1]_{4\times4} & [M_2]_{4\times4} \\ [M_3]_{4\times4} & [M_4]_{4\times4} \end{bmatrix} \begin{Bmatrix} [y_1]_{4\times1} \\ [y_2]_{4\times1} \end{Bmatrix} = \vec{0} \tag{30}$$

where

$$\hat{M}_1 = \begin{bmatrix} -\lambda^3 & \alpha_{11}(1+i\eta_{11}) & \lambda^3 & \alpha_{11}(1+i\eta_{11}) \\ -\alpha_{10}(1+i\eta_{10}) & -\lambda & -\alpha_{10}(1+i\eta_{10}) & \lambda \\ -\sin(\lambda) & -\cos(\lambda) & \sinh(\lambda) & \cosh(\lambda) \\ -\lambda^3\cos(\lambda) - \Lambda_1\mu_{11}\sin(\lambda) & \lambda^3\sin(\lambda) - \Lambda_1\mu_{11}\cos(\lambda) & \lambda^3\cosh(\lambda) - \Lambda_1\mu_{11}\sinh(\lambda) & \lambda^3\sinh(\lambda) - \Lambda_1\mu_{11}\cosh(\lambda) \end{bmatrix}$$

$$\hat{M}_2 = \begin{bmatrix} 0 & 0 & 0 & 0 \\ 0 & 0 & 0 & 0 \\ 0 & 0 & 0 & 0 \\ -\Lambda_1\mu_{12}\sin(\lambda) & -\Lambda_1\mu_{12}\cos(\lambda) & -\Lambda_1\mu_{12}\sinh(\lambda) & -\Lambda_1\mu_{12}\cosh(\lambda) \end{bmatrix}$$

$$\hat{M}_3 = \begin{bmatrix} 0 & 0 & 0 & 0 \\ 0 & 0 & 0 & 0 \\ 0 & 0 & 0 & 0 \\ -\Lambda_1\mu_{21}\sin(\lambda) & -\Lambda_1\mu_{21}\cos(\lambda) & -\Lambda_1\mu_{21}\sinh(\lambda) & -\Lambda_1\mu_{21}\cosh(\lambda) \end{bmatrix}$$

$$\hat{M}_4 = \begin{bmatrix} -\lambda^3 & \alpha_{21}(1+i\eta_{21}) & \lambda^3 & \alpha_{21}(1+i\eta_{21}) \\ -\alpha_{20}(1+i\eta_{20}) & -\lambda & -\alpha_{20}(1+i\eta_{20}) & \lambda \\ -\sin(\lambda) & -\cos(\lambda) & \sinh(\lambda) & \cosh(\lambda) \\ -\lambda^3\cos(\lambda) - \Lambda_1\mu_{22}\sin(\lambda) & \lambda^3\sin(\lambda) - \Lambda_1\mu_{22}\cos(\lambda) & \lambda^3\cosh(\lambda) - \Lambda_1\mu_{22}\sinh(\lambda) & \lambda^3\sinh(\lambda) - \Lambda_1\mu_{22}\cosh(\lambda) \end{bmatrix}$$

$$\vec{y}_1^{\,T} = \{A_1 \quad B_1 \quad C_1 \quad D_1\}, \quad \vec{y}_2^{\,T} = \{A_2 \quad B_2 \quad C_2 \quad D_2\}$$

In order to have nontrivial solution for Eq. (30), the determinant of coefficient matrix must be equal to zero. Expansion of this determinant leads to the following complex characteristic equation:

$$a\Lambda_1^2 + b\Lambda_1 + c = 0 \tag{31}$$

The coefficients a–c are complex value terms; hence, in general, solution of (31) is a complex value. Substituting Λ_0 from (21) into (7), the axial cut depth at stability boundaries can be obtained as follows:

$$b_{\lim} = -\frac{EI}{K_s L^3}\frac{\Lambda_1}{1-e^{-i\omega\tau}} \tag{32}$$

Replacing Λ_1 and $e^{-i\omega\tau}$ with $\Lambda_1 = \Lambda_{1R}+i\Lambda_{1I}$ and $e^{-i\omega\tau} = \cos(\omega\tau)-i\sin(\omega\tau)$, respectively, one arrives at

$$b_{\lim} = -\frac{EI}{K_s L^3}\left\{\frac{\Lambda_{1R}\left(1-\cos(\omega\tau)\right) + \Lambda_{1I}\sin(\omega\tau)}{(1-\cos(\omega\tau))^2+\sin^2(\omega\tau)} + i\frac{\Lambda_{1I}(1-\cos(\omega\tau)) - \Lambda_{1R}\sin(\omega\tau)}{(1-\cos(\omega\tau))^2+\sin^2(\omega\tau)}\right\} \tag{33}$$

$b_{\lim}$ is a real-value term; hence, the imaginary part of (33) must vanish:

$$\Lambda_{1I}(1-\cos(\omega\tau)) - \Lambda_{1R}\sin(\omega\tau) = 0 \tag{34}$$

or

$$\kappa = \frac{\Lambda_{1R}}{\Lambda_{1I}} = \frac{1-\cos(\omega\tau)}{\pm\sqrt{1-\cos^2(\omega\tau)}} \tag{35}$$

The trivial solution of (34) is $\omega\tau = 0+2m\pi$, which corresponds to the no-chatter case. The nontrivial solution is as follows:

$$\cos(\omega\tau) = \frac{1-\kappa^2}{1+\kappa^2} \tag{36}$$

or

$$\omega\tau = 2m\pi + \cos^{-1}\left(\frac{1-\kappa^2}{1+\kappa^2}\right)$$
$$\omega\tau = 2(m+1)\pi - \cos^{-1}\left(\frac{1-\kappa^2}{1+\kappa^2}\right), \qquad m = 0,1,2,\ldots \tag{37}$$

Eq. (37) defines the relationship between chatter frequency and tooth-passing frequency. Substituting (36) into (33), the imaginary part of (33) vanishes and the following equation for $b^{\lim}$ is obtained:

$$b_{\lim} = -\frac{EI\Lambda_{1I}}{2K_s L^3}(\kappa + (1/\kappa)) \quad \text{or}$$
$$b_{\lim} = -\frac{EI}{2K_s L^3 \Lambda_{1R}}(\Lambda_{1R}^2 + \Lambda_{1I}^2) \tag{38}$$

Finally the stability lobes are obtained by following steps:

Step1: Selecting M different chatter frequencies around the tool dominant mode.

Step2: Selecting N integer values for m in (37) to evaluate N stability lobes.

Step3: Determining the stability limit from (38) at each chatter frequency.

Step4: Determining the corresponding tooth-passing period from Eq. (37).Elastic support parameters in the continuous model are identified in the following section.

4. Identification of tool/holder/spindle interface parameters

The elastic support parameters in the continuous model are identified with the aid of an impact hammer test. The cutting tool is simulated by a 20 mm diameter test bar that is mounted in a collet-type holder with an overhang of 208 mm. The tool tip FRFs of the test bar in feed and perpendicular directions are shown in Fig. 2. The extracted modal frequency ω_n, modal damping ζ, and modal residue for the first two modes in feed (X) and perpendicular (Y) directions are tabulated in Table 1.

Due to axial symmetry of the tool and tool/holder/spindle interface it is sufficient to identify the elastic support parameters in one direction such as feed direction (Fig. 1b). Using extracted modal parameters of the experimental setup in Table 1, identification of

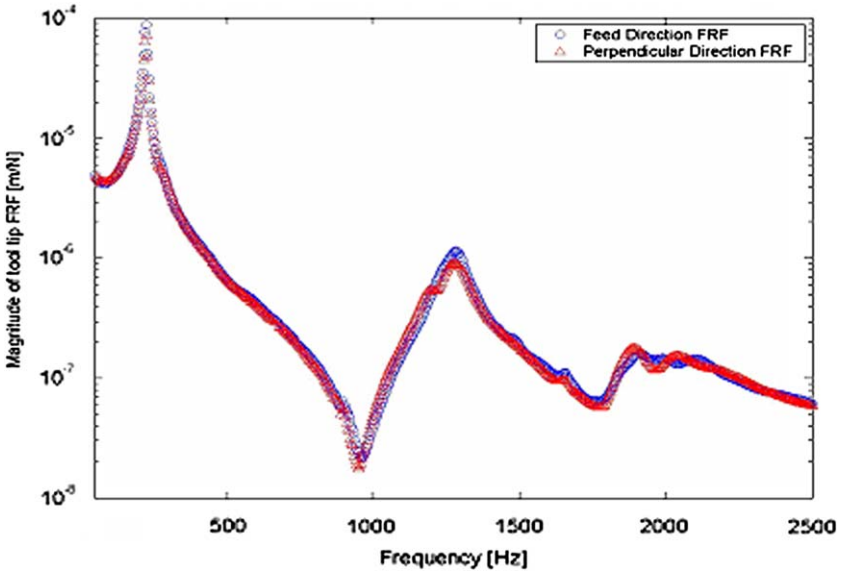

Fig. 2. Magnitude of tool tip FRF in X and Y directions.

elastic support parameters in the continuous model is done in two steps.

4.1. Identification of stiffness parameters (α_{11} and α_{10})

In order to identify the stiffness parameters of elastic support, un-damp model of the structure and un-damp natural frequencies are used. As shown in Table 1, modal damping factors are small (less than three percent), so the structure is a lightly damped one and un-damped natural frequencies are approximately same as damped ones. Omitting hysteretic damping factors (η_{10}, η_{11}) and milling force (F_1) from boundary conditions in (19), the un-damped model in feed (X) direction is obtained as follows:

$$\begin{aligned} &w_1^{\mathrm{iv}} + \ddot{w}_1 = 0 \\ &w_1'''(0,t) + \alpha_{11} w_1(0,t) = 0, \quad w_1''(0,t) - \alpha_{10} w_1'(0,t) = 0 \\ &w_1'''(1,t) = 0, \qquad\qquad w_1''(1,t) = 0 \end{aligned} \tag{39}$$

Separating the variables, one arrives at the following ordinary differential equation:

$$\begin{aligned} &\varphi^{\mathrm{iv}} - \lambda^4 \varphi = 0 \\ &\varphi'''(0) + \alpha_{11}\varphi(0) = 0, \quad \varphi''(0) - \alpha_{10}\varphi'(0) = 0 \\ &\varphi'''(1) = 0, \varphi''(1) = 0 \end{aligned} \tag{40}$$

Eq. (26) must satisfy the boundary conditions set in (40). Rewriting these equations in matrix form one arrives at

$$\hat{U}_1 \vec{q}_1 = 0 \tag{41}$$

where

$$\hat{U}_1 = \begin{bmatrix} -\lambda^3 & \alpha_{11} & \lambda^3 & \alpha_{11} \\ \alpha_{10} & \lambda & \alpha_{10} & -\lambda \\ -\sin(\lambda) & -\cos(\lambda) & \sinh(\lambda) & \cosh(\lambda) \\ -\cos(\lambda) & \sin(\lambda) & \cosh(\lambda) & \sinh(\lambda) \end{bmatrix}, \quad \vec{q}_1 = \begin{bmatrix} A_1 \\ B_1 \\ C_1 \\ D_1 \end{bmatrix}$$

In order to have a nontrivial solution for Eq. (41), the determinant of coefficient matrix $\hat{U}_1$must be equal to zero. Expansion of this determinant leads to a characteristic equation, which is a function of λ, α_{10}, and α_{11}. Replacing λ with damped natural frequencies in feed (X) direction (Table 1), using $\lambda^4 = \omega^2$, and following Eq. (42) to obtain non-dimensional frequencies, one arrives at two non-linear equations.

Table 1
Extracted modal parameters of the experimental setup.

Direction	Mode	ω_n (Hz)	ζ (%)	Mode residue (m/N)(rad/s)
X	1	222	1.70	$(42.0-i\times 11.0)\times 10^{-4}$
	2	1280	2.84	$(4.78-i\times 1.56)\times 10^{-4}$
Y	1	222	2.02	$(40.0-i\times 13.0)\times 10^{-4}$
	2	1290	3.27	$(3.36-i\times 2.51)\times 10^{-4}$

$$\omega = \sqrt{\frac{mL^4}{EI}}\omega_{n[\frac{\mathrm{rad}}{\mathrm{s}}]} \tag{42}$$

After solving the equations simultaneously, the elastic support stiffness parameters are obtained as $\alpha_{11} = 102.6218$ and $\alpha_{10} = 3.6913$. The next step is to identify the damping parameters.

4.2. Identification of damping parameters (η_{10} and η_{11})

In order to identify the damping parameters of elastic support, the following damped model of the structure is used:

$$w_1^{\mathrm{iv}} + \ddot{w}_1 = 0 \tag{43}$$

$$\begin{aligned} &w_1'''(0,t) + (1+i\eta_{11})\alpha_{11} w_1(0,t) = 0, \\ &w_1''(0,t) - (1+i\eta_{10})\alpha_{10} w_1'(0,t) = 0 \\ &w_1'''(1,t) = 0, \quad w_1''(1,t) = 0 \end{aligned} \tag{44}$$

Separating the variables in (43), one arrives at

$$\ddot{T} - ST = 0 \tag{45}$$

$$\varphi^{\mathrm{iv}} + S\varphi = 0 \tag{46}$$

For the presence of damping, eigenvalues of system (S) are complex numbers with negative real part. Hence, time domain function (T) is as follows:

$$T(t) = e^{-\sigma t}\{A_0\cos(\omega t) + B_0\sin(\omega t)\}, \quad \sigma, \omega > 0 \tag{47}$$

Substituting (47) into (45), one obtains the following matrix form equation:

$$\begin{bmatrix} \sigma^2-\omega^2-S & -2\sigma\omega \\ 2\sigma\omega & \sigma^2-\omega^2-S \end{bmatrix} \begin{Bmatrix} A_0 \\ B_0 \end{Bmatrix} = \vec{0} \tag{48}$$

To have a nontrivial solution for Eq. (48), the determinant of coefficient matrix must be equal to zero, which yields

$$S = (\sigma^2-\omega^2) \pm 2\sigma\omega i \tag{49}$$

Substituting (49) into (46) and assuming e^{rx} as a solution of (46), one arrives at

$$r^4 = (\omega^2-\sigma^2) + 2\sigma\omega i \tag{50}$$

$$r^4 = (\omega^2-\sigma^2) - 2\sigma\omega i \tag{51}$$

Solving (50) and (51) with respect to r yields two eigenvectors $\varphi^+(x)$ and $\varphi^-(x)$, respectively. Rewriting the right hand side of (50) in polar form, one obtains

$$r^4 = (\omega^2-\sigma^2) + 2\sigma\omega i = Re^{i(2m\pi+\Omega^+)}, \quad m = 0, \pm1, \pm2, \cdots \tag{52}$$

where

$$R = \sqrt{(\omega^2-\sigma^2)^2 + 4\sigma^2\omega^2}, R \geq 0 \tag{53}$$

$$\Omega^+ = \tan^{-1}\left(\frac{2\sigma\omega}{\omega^2-\sigma^2}\right), \quad 0 \leq \Omega^+ \leq \frac{\pi}{2} \tag{54}$$

Hence

$$r = R^{0.25}e^{i((\Omega^+/4)+((m\pi)/2))} = R^{0.25}\left\{\cos\left(\frac{\Omega^+}{4}+\frac{m\pi}{2}\right) + i\sin\left(\frac{\Omega^+}{4}+\frac{m\pi}{4}\right)\right\} \tag{55}$$

Setting m equal to 0, 1, 2, and 3, four different values of r are obtained. For other values of m, answers will be repeated. Therefore

$$\varphi^+(x) = A_3e^{(\delta^+ + i\gamma^+)x} + B_3e^{(-\gamma^+ + i\delta^+)x} + C_3e^{(-\delta^+ - i\gamma^+)x} + D_4e^{(\gamma^+ - i\delta^+)x} \tag{56}$$

where

$$\delta^+ = R^{0.25}\cos\left(\frac{\Omega^+}{4}\right), \quad \gamma^+ = R^{0.25}\sin\left(\frac{\Omega^+}{4}\right) \tag{57}$$

σ and ω are positive and $\sigma<\omega$ for lightly damped system. Hence, $(\omega^2-\sigma^2)-2\sigma\omega i$ is in the fourth region of complex plane and its polar form is $Re^{i(2m\pi+\Omega^-)}$, where $\Omega^- = 2\pi-\Omega^+$. R and Ω^+ have been defined in (53) and (54), respectively. Following the same approach for obtaining $\varphi^+(x)$, one arrives at

$$\varphi^-(x) = A_4e^{(\delta^- + i\gamma^-)x} + B_4e^{(-\gamma^- + i\delta^-)x} + C_4e^{(-\delta^- - i\gamma^-)x} + D_4e^{(\gamma^- - i\delta^-)x} \tag{58}$$

where

$$\delta^- = R^{0.25}\sin\left(\frac{\Omega^+}{4}\right), \quad \gamma^- = R^{0.25}\cos\left(\frac{\Omega^+}{4}\right) \tag{59}$$

Both $\varphi^+(x)$ and $\varphi^-(x)$ are eigenvectors of the system and they satisfy boundary conditions set in (44). By separating the variables and rewriting these equations in matrix form, one obtains:

$$\hat{U}_2\vec{q}_2 = 0 \tag{60}$$

where

$$\hat{U}_2 = \begin{bmatrix} (\delta^+ + i\gamma^+)^3 + (1+i\eta_{11})\alpha_{11} & (-\gamma^+ + i\delta^+)^3 + (1+i\eta_{11})\alpha_{11} & (-\delta^+ - i\gamma^+)^3 + (1+i\eta_{11})\alpha_{11} & (\gamma^+ - i\delta^+)^3 + (1+i\eta_{11})\alpha_{11} \\ (\delta^+ + i\gamma^+)^2 - (1+i\eta_{10})\alpha_{10}(\delta^+ + i\gamma^+) & (-\gamma^+ + i\delta^+)^2 - (1+i\eta_{10})\alpha_{10}(-\gamma^+ + i\delta^+) & (-\delta^+ - i\gamma^+)^2 - (1+i\eta_{10})\alpha_{10}(-\delta^+ - i\gamma^+) & (\gamma^+ - i\delta^+)^2 - (1+i\eta_{10})\alpha_{10}(\gamma^+ - i\delta^+) \\ (\delta^+ + i\gamma^+)^2e^{(\delta^+ + i\gamma^+)} & (-\gamma^+ + i\delta^+)^2e^{(-\gamma^+ + i\delta^+)} & (-\delta^+ - i\gamma^+)^2e^{(-\delta^+ - i\gamma^+)} & (\gamma^+ - i\delta^+)^2e^{(\gamma^+ - i\delta^+)} \\ (\delta^+ + i\gamma^+)^3e^{(\delta^+ + i\gamma^+)} & (-\gamma^+ + i\delta^+)^3e^{(-\gamma^+ + i\delta^+)} & (-\delta^+ - i\gamma^+)^3e^{(-\delta^+ - i\gamma^+)} & (\gamma^+ - i\delta^+)^3e^{(\gamma^+ - i\delta^+)} \end{bmatrix}$$

$$\vec{q}_2^{\,T} = \begin{bmatrix} A_3 & B_3 & C_3 & D_3 \end{bmatrix}$$

In order to have a nontrivial solution for Eq. (60), the determinant of coefficient matrix, $\hat{U}_2$, must be equal to zero. Expansion of this determinant leads to a complex characteristic equation, which is a function of δ, γ, η_{10}, and η_{11}. Equating the real and imaginary parts of the characteristic equation to zero, one obtains two nonlinear

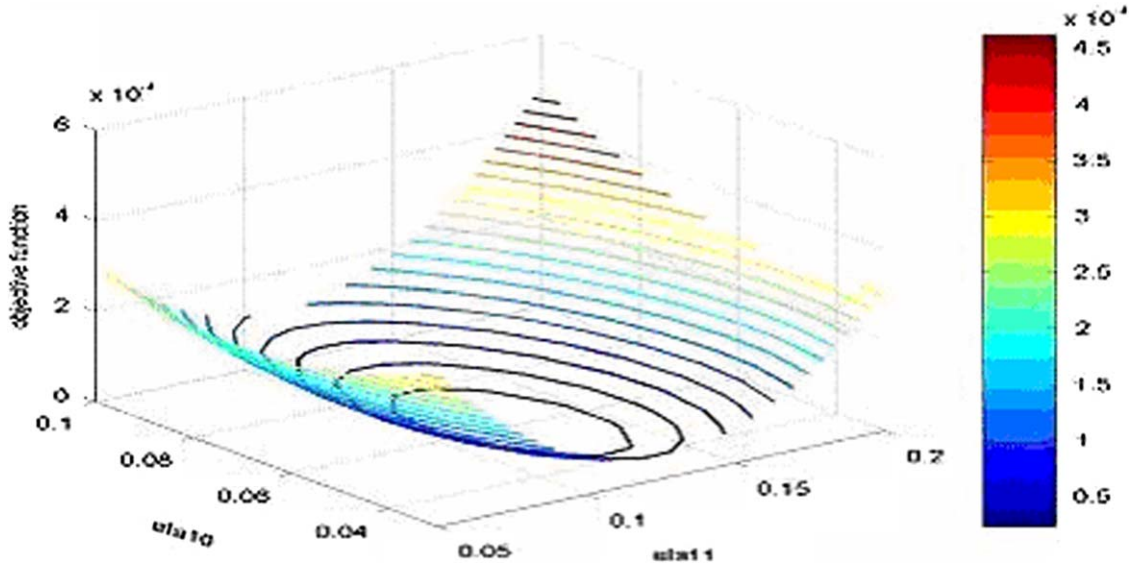

Fig. 3. Contour plot of the objective function.

equations. Using these equations and least-squares optimization method, η_{10} and η_{11} are identified. For different points in the η_{10}–η_{11} plane, solving the obtained set of nonlinear equations yields corresponding δ and γ, which are converted to R and Ω^+ through (57) and then to σ and ω through (53) and (54). Desired values of η_{10} and η_{11} must minimize the following objective function:

$$\Gamma = \sum_{j=1}^{2}\left[\left(\frac{\sigma_{jE}-\sigma_{jC}}{\sigma_{jE}}\right)^2+\left(\frac{\omega_{jE}-\omega_{jC}}{\omega_{jE}}\right)^2\right] \tag{61}$$

Here σ_j and ω_j are the real and imaginary parts of the jth eigenvalue, respectively. Subscript E represents eigenvalues obtained from impact tests and modal analysis for experimental setup and subscript C represents eigenvalues obtained from calculations for the elastic support model. Fig. 3 shows contour plots of the objective function. For $\eta_{11}=0.12$ and $\eta_{10}=0.06$ the objective function (Γ) is minimum. Repeating the identification procedure using other eigenvectors in (58) results in the same values for η_{10} and η_{11}.

The following section employs the proposed procedure and identified elastic support beam model parameters to obtain the stability lobes.

5. Experimental simulation

In order to verify the performance of the proposed method in obtaining stability lobes and comparing results with those obtained from the lumped-parameter method a simulated case study is performed. In this study a long slender end mill in slotting operation is simulated by a test bar introduced in Section 4. The specifications of elastic support beam model of this experimental setup in feed and perpendicular directions are tabulated in Table 2. The workpiece material is aluminium ($K_s=700$ MPa). Using Eqs. (37) and (38) the stability lobes are computed and are shown in Fig. 4.

Table 2
Tool, support, and workpiece properties.

E (GPa)	207	No. of flutes	2
ρ (kg/m^3)	7860	Tool dia. (m)	0.02
K_s (MPa)	700	Tool length (m)	0.208
α_{10}	3.6913	η_{10}	0.06
α_{11}	102.6518	η_{11}	0.12
α_{20}	3.6913	η_{20}	0.06
α_{21}	102.6518	η_{21}	0.12

Next the stability lobes are determined using the lumped-parameter method presented by Budak and Altintas [4]. In this method the frequency response of the tool/spindle assembly at the tool tip is required, which is measured by impact test and extracted modal parameters for the first two modes of the system in feed and perpendicular directions are tabulated in Table 1. The stability lobes obtained using the lumped-parameter method are also presented in Fig. 4. Comparing the results obtained from both methods, one observes a good agreement between the results. The predictions of the continuous model are conservative compared to the lumped-parameter model, i.e. the prediction for critical depth of cut is lower in the new method. This can be explained noticing the fact that the lumped-parameter model presents a less accurate model of the system using only few modes while in the continuous model all modes participate in the response. Hence by an accurate representation of the system the proposed model provide a more accurate model of the system.

6. Conclusions

Long, slender end mills are often used in automotive, biomedical, and aerospace industries for macro- or micro-machining of various components. It is known that most of the deflections encountered during machining with these tools are concentrated in the tool and tool/holder interface. A continuous model comprised of an Euler–Bernoulli beam to represent the tool and a set of translational and torsional springs and dampers to represent the tool–holder interface is proposed to predict the stability lobes. Since interface parameters do not change when the tool length is altered in tool-tuning practice, the need for FRF measurement for each tool length will be

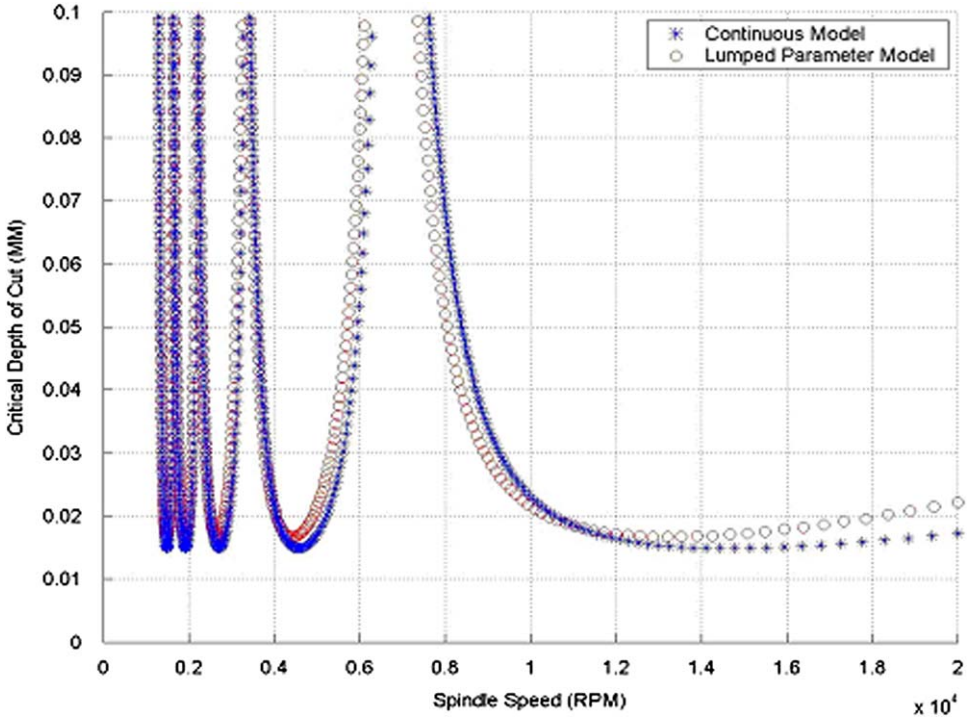

Fig. 4. Predicted stability lobes by the continuous and lumped-parameter models.

omitted, especially in micro-machining, using the continuous model in predicting stability lobes. Moreover, this model is an effective tool to study the influence of micro-slip, as a nonlinear effect, at the interface between tool/holder, on chatter vibrations.

The stability analysis of the derived continuous model formulation is done in frequency domain using the single-frequency solution method. Although, this method is efficient and accurate in high radial immersion case such as slotting, which is considered in this study, its accuracy decreases with decreasing radial immersion. Low radial immersion milling bears a new type of instability called flip bifurcation or periodic chatter in addition to the already well-known type named Hopf bifurcation or quasi-periodic chatter. The stability analysis of continuous model formulation using time domain approaches for low immersion cuts is a promising topic for future work. The impact hammer test is used to identify the stiffness and damping parameters of the tool/holder/spindle interface.

The stability lobes' derivation using the lumped-parameter model for high radial immersion is a well-researched topic and is proven through considerable experiments by different researchers in the past. Stability lobes obtained by the continuous model formulation are compared with the lumped-parameter model lobes. There is a good agreement between the two results with a very small difference, which validates the continuous model. Besides, continuous model lobes are on the conservative side, even though to a small amount, but still it can speak on the fact that considering all participating modes in responses by the continuous model makes it a more accurate model in comparison with the lumped-parameter model.

References

[1] J. Tlusty, Dynamics of high-speed milling, ASME Journal of Engineering for Industry 108 (1986) 59–67.

[2] S. Smith, J. Tlusty, Update on high-speed milling dynamics, ASME Journal of Engineering for Industry 112 (1990) 142–149.

[3] I. Minis, R. Yanushevsky, A new theoretical approach for the prediction of machine tool chatter in milling, ASME Journal of Engineering for Industry 115 (1993) 1–8.

[4] E. Budak, Y. Altintas, Analytical prediction of chatter stability in milling—parts I and II, ASME Journal of Dynamic Systems, Measurement, and Control 120 (1998) 22–36.

[5] M.A. Davies, J.R. Pratt, B. Dutterer, T.J. Burns, Stability prediction for low radial immersion milling, ASME Journal of Manufacturing Science and Engineering 124 (2002) 217–225.

[6] P.V. Bayly, J.E. Halley, B.P. Mann, M.A. Davies, Stability of interrupted cutting by temporal finite element analysis, ASME Journal of Manufacturing Science and Engineering. 125 (2003) 220–225.

[7] T. Insperger, B.P. Mann, G. Stepan, P.V. Bayly, Stability of up-milling and down-milling—parts 1 and 2, International Journal of Machine Tools and Manufacture 43 (2003) 25–40.

[8] T. Insperger, G. Stepan, P.V. Bayly, B.P. Mann, Multiple chatter frequencies in milling processes, Journal of Sound and Vibration 262 (2003) 333–345.

[9] T. Insperger, G. Stepan, Updated semi-discretization method for periodic delay—differential equations with discrete delay, International Journal of Numerical Methods in Engineering 61 (2004) 117–141.

[10] T. Insperger, G. Stepan, Vibration frequencies in high-speed milling processes or a positive answer to Davies, Pratt, Dutterer and Burns, ASME Journal of Manufacturing and Engineering 126 (2004) 481–487.

[11] E. Budak, A. Tekeli, Maximizing chatter free material removal rate in milling through optimal selection of axial and radial depth of cut pairs, CIRP Annals—Manufacturing Technology 54 (2005) 353–356.

[12] E. Govekar, J. Gradisek, M. Kalveram, T. Insperger, K. Weinert, G. Stepan, I. Grabec, On stability and dynamics of milling at small radial immersion, CIRP Annals—Manufacturing Technology 54 (2005) 357–362.

[13] J. Gradisek, M. Kalveram, T. Insperger, K. Weinert, G. Stepan, E. Govekar, I. Grabec, On stability prediction for milling, International Journal of Machine Tools and Manufacture 45 (2005) 769–781.

[14] T. Insperger, B.P. Mann, T. Surmann, G. Stepan, On the chatter frequencies of milling processes with runout, International Journal of Machine Tools and Manufacture 48 (2008) 1081–1089.

[15] R.G. Landers, A.G. Ulsoy, Nonlinear feed effect in machining chatter analysis, ASME Journal of Manufacturing Science and Engineering 130 (2008) 011017–011018.

[16] M. Davies, B. Dutterer, J. Pratt, A. Schaut, On the dynamics of high-speed milling with long, slender endmills, Annals of CIRP 47 (2) (1998) 55–60.

[17] J. Chae, S.S. Park, T. Freiheit, Investigation of micro-cutting operations, International Journal of Machine Tools and Manufacture 46 (2006) 313–332.

[18] B.A. Mascardelli, S.S. Park, T. Freiheit, Substructure coupling of microend mills to aid in the suppression of chatter, ASME Journal of Manufacturing Science and Engineering 130 (2008) 011010–011112.

[19] T.L. Schmitz, Predicting high-speed machining dynamics by substructure analysis, Annals of CIRP 49 (2000) 303–308.

[20] T.L. Schmitz, M.A. Davies, K. Medicus, J. Synder, Improving high-speed machining material removal rates by rapid dynamic analysis, Annals of CIRP 50 (2001) 263–268.

[21] T.L. Schmitz, M.A. Davies, M.D. Kennedy, Tool point frequency response prediction for high-speed machining by RCSA, ASME Journal of Manufacturing Science and Engineering 123 (2001) 700–707.

[22] T.L. Schmitz, T.J. Burns, J.C. Ziegert, Tool length dependent stability surfaces, Machining Science and Technology 8 (2004) 377–397.

[23] E. Budak, A. Erturk, H.N. Ozguven, A modeling approach for analysis and improvement of spindle–holder–tool assembly dynamics, CIRP Annals—Manufacturing Technology 55 (2006) 369–372.

[24] M. Namazi, Y. Altintas, T. Abe, N. Rajapakse, Modeling and identification of tool holder–spindle interface dynamics, International Journal of Machine Tools and Manufacture 47 (2007) 1333–1341.

[25] S. Filiz, C.H. Cheng, K.B. Powell, T.L. Schmitz, O.B. Ozdoganlar, An improved tool-holder model for RCSA tool-point frequency response prediction, Precision Engineering 33 (2009) 26–36.